Research Article ISSN 2771-666X

Journal of Advanced Materials Science and Engineering

Integrated Approach at the Process-Property-Performance Nexus to Characterizing Process-Induced Properties and Behavior of Additively Manufactured Thermoplastic Polymers

Ahmed Sherif El-Gizawy[1,2,3,4,*], Ammar A. Melaibari[3] and George Youssef[1]

[1]*Department of Mechanical Engineering, San Diego State University, San Diego, California 92182, USA.*

[2]*Mechanical and Aerospace Engineering, University of Missouri-Columbia, Columbia, Missouri 65201, USA.*

[3]*Mechanical Engineering Department, Center of Nanotechnology, King Abdulaziz University, Jeddah 21589, Saudi Arabia.*

[4]*Industrial Technology Development and Management, (ITECH D&M), LLC, Columbia, Missouri 65203, USA.*

[*]Correspondence:
Ahmed Sherif El-Gizawy, Department of Mechanical Engineering, San Diego State University, San Diego, California 92182, USA.

Received: 11 Dec 2023; **Accepted:** 13 Jan 2024; **Published:** 20 Jan 2024

Citation: El-Gizawy AS, Melaibari AA, Youssef G. Integrated Approach at the Process-Property-Performance Nexus to Characterizing Process-Induced Properties and Behavior of Additively Manufactured Thermoplastic Polymers. J Adv Mater Sci Eng. 2024; 4(1): 1-10.

ABSTRACT

Material extrusion (MEX) is an additive manufacturing process to fabricate prototypes using thermoplastic polymers. As this additive manufacturing technology continues to mature from a rapid prototyping process to a rapid manufacturing technique, predicting the mechanical behavior of 3D printed parts using representative models becomes essential for translating products quickly from bench to market. Predictive models allow product designers to accurately forecast mechanical performance while reducing the overall design cycle and reliance on costly physical experimentations. This research presents an integrated approach at the process-property-performance nexus to characterizing process-induced properties and effectively utilizing the measured properties within a predictive analysis framework tailored to design MEX-printed products. To this end, two methods were investigated leveraging the anisotropy of additively manufactured parts. The first method involved using finite element simulations to separate the part into bonded layers corresponding to 3D printed layers and individually applying the raster angles to each layer. The second method employed the classical lamination theory, ubiquitous in the analysis of laminated composite materials, to calculate effective, homogenized properties based on the number and orientation of the layers. Using individual cells in finite element software to represent layers and averaging layer properties has proven effective in modeling MEX parts for stress analysis. Case studies using MEX-printed ULTEM 9085 structures are presented to verify the effectiveness of developed models. The results provide a practical design pathway to shorten the development cycle and accelerate the deployment of additively manufactured parts in load-bearing scenarios.

Keywords
Additive manufacturing, Material extrusion, Thermoplastic polymers, ULTEM 9085, Process-induced properties, Finite element modeling, Classical laminate theory, Predictive design models.

Introduction
Three-dimensional (3D) printing by material extrusion (MEX) is a manufacturing process that creates parts by depositing molten polymer filaments in successive layers (see Figure 1) [1,2]. This process is also commonly recognized by several names according to ASTM F3529-21, including Fused Filament Fabrication (FFF)

and Fusion Deposition Modeling (FDM). Abiding with ASTM terminology for additive manufacturing processes, MEX is used throughout this report in lieu of the other common abbreviations. The most basic, and arguably the most common, MEX additive manufacturing process is based on a gantry motion system. However, other motion systems have also been adopted in MEX additive manufacturing equipment, including robotics and delta machines. The focus herein is on MEX processing with a traditional gantry system. The polymer filament is fed through an extrusion nozzle that heats the filament to a semi-molten state. The extrusion and heating assembly is mounted on a gantry motion system that helps strategically deposit the molten filaments on the build platform or plate [3-9]. The plate then moves within a temperature-controlled printing chamber along the z-axis to allow the deposition of the next layer upon the previous layer. The variety of materials available, ease of producing complex geometries, and fast fabrication times make MEX an attractive manufacturing process for several engineering domains, including the biomedical and aerospace industries, to name a few prominent examples [10-13]. As the demand for 3D printed parts in end-use applications has increased, it has become essential to devise an integrated framework to structurally analyze such parts, *i.e.*, leading to the digital twin [14,15]. Virtual experimentations can reduce the development cycle and accelerate deployment into load-bearing scenarios, a common need in various industries. Example applications include virtual crashworthiness assessment for carmakers or wind tunnel testing for aircraft developers. Efforts are underway to develop fully integrated computational methods to eliminate the current heuristic design process, including the design-build-test approach, and promising substantial cost, time, and effort savings.

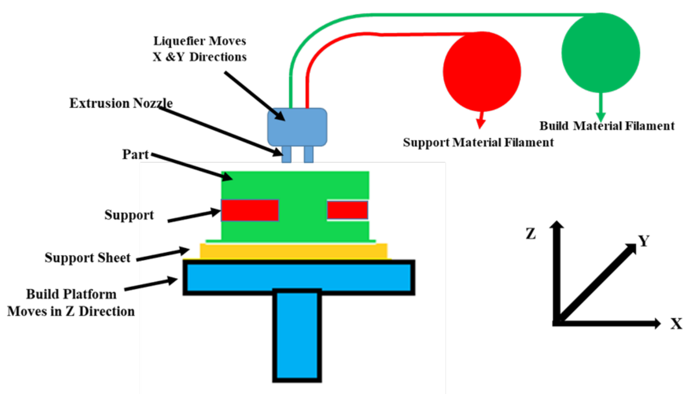

Figure 1: Schematic of materials extrusion (MEX) additive manufacturing system used for 3D printing parts by feeding a polymer filament into heated extrusion nozzle and depositing the molten filament strategically based on the part geometry.

Much work has already been accomplished toward predictive modeling of the mechanical response of MEX-fabricated parts and components. Previous research highlighted the importance of several process parameters, including extrusion pattern, part size, road gap, extrusion temperature, and oven temperature, on the mechanical performance of the final 3D printed samples using the MEX process (*e.g.*, stiffness and strength) [16-19]. Youssef et al. reported novel developments in improving the functionality of polymer-based parts fabricated by the MEX method [20,21]. They added electrical conductivity and fluid management to the existing load-bearing capabilities of the MEX-printed parts. Youssef et al. also used finite element modeling to identify the areas of structural weaknesses and assist in elucidating the failure modes of the printed parts [20,21]. More recent efforts have been applied to determine residual stress in MEX-printed parts caused by the thermal cycling experienced by filaments during deposition [22,23], which is valuable but falls short in forecasting the performance in service loading conditions. The primary outcomes of previous research demonstrate the necessity for predictive models to elucidate the processing-property-performance interrelationship of MEX-printed components.

Other established analysis tools, including classical laminate theory (CLT), have also been applied to MEX parts to predict the mechanical response to applied loads [16,22-24]. These tools are valid since MEX-printed parts closely resemble laminate composite structures with filaments, or raster, analogous to composite fibers. The similarity of composite laminates to MEX parts also extends to the process-induced anisotropy intrinsic to MEX [25-28]. This makes the classical laminate theory a convenient analysis tool to readily account for material anisotropy and layer orientation that affect the mechanical properties of a specific layer and the entire part. For example, the elastic constants required to describe the constitutive response of the MEX-printed materials include E_1, E_2, and E_3, representing Young's moduli of a layer along the principal axes, G_{12}, G_{13}, and G_{23} are the shear moduli, and υ_{12}, υ_{13}, and υ_{23} are the Poisson's ratios.

Shah et al. [29] utilized an indigenously built nozzle attachment with the MEX process to characterize tensile properties for newly developed continuous glass fiber–reinforced thermoplastic composite products. Their results show that the tensile strength of glass fiber–reinforced composites was 218% to 241% greater than that of just thermoplastic specimens when the printing raster direction was 0° and 35% to 45% lower when the printing raster orientation was 90°. Hyatt et al. [30] presented the design of coupons and test methodology for orthotropic characterization of MEX-processed ULTEM 9085. Three sets of coupons were fabricated and tested based on the improved coupon design and test methodologies to report the tensile, compression, and shear properties in X, Y, and Z directions - for pure contour and pure raster constructions. Özen et al. [31] proposed a computational homogenization approach for obtaining the effective properties of the MEX-related anisotropic structure. Their approach involved a systematic methodology for acquiring the anisotropy from the process-related inner substructure (microscale) to the material response at the homogenized length scale (macroscale). Özen et al. [32] extended their practical approach to simulating the mechanical properties of MEX-printed fiber-reinforced polymer composites. They predicted homogenized material properties for different composites by asymptotic homogenization at the microscale. Uniaxial tensile test simulations were performed through finite element methods (FEM). They claim that transverse isotropic material properties were observed except for the composite materials with random particle orientations [31]. They proposed the generation of different symmetry axes for the characterization of transverse isotropic materials. Both investigations did not reveal any reliable stiffness properties of the printed composites that can be used with FEM for simulating the behavior of the printed products under service loading conditions [31,32].

Enrique et al. [33] extensively reviewed experimental characterization and predictive models for evaluating MEX process-induced properties. This review concluded that no single approach can be used individually; instead, a combination of characterization tools should be considered for a reliable property estimation. Common to all current investigations [25-32] is using CLT to predict the behavior of printed materials, assuming that individually printed layers exhibit transversely isotropic. This assumption results in $E_3 = E_2$, $\upsilon_{13} = \upsilon_{12}$, and inaccurately resolving shear moduli from uniaxial testing.

The present work addresses the above-mentioned problems and presents an integrated approach for the characterization of process-induced properties of MEX printed materials and effectively applying these properties to novel predictive analysis methods for designing functionally printed products.

Integrated Approach

The integrated approach used to develop predictive models for designing MEX-manufactured products is displayed in Figure 2. First, data on the mechanical performance of MEX-processed samples with different raster angles and build orientations is collected. The raster angle is defined as the direction of the molten filaments deposited on the build plate. The build orientation is the direction in which the entire part is printed. The data consists of stiffness and strength properties along the three principal axes obtained by specially designed tension tests. Shear stiffness properties are obtained using standard shear testing for composite materials. An integrative analysis leveraging the classical laminate theory and the extracted experimental data is used in this work to determine the anisotropic stiffness matrix for MEX-based parts. All results were then used to establish constitutive relationships combined with finite elements analysis to design MEX-based structures for strength and stiffness.

Two methods were developed to perform finite element analyses of the MEX parts, exploiting the similarities of MEX-printed parts and laminated composite structures by accounting for the orientations of individual layers. The first method, referred to as the layered method, accomplished by employing the features of finite element software ANSYS to partition the parts into cells representing each MEX layer, and applying the layer orientation to each cell. The second method, termed the bulk properties method, used the laminate theory to determine the effective (or averaged) properties and applied the global averaged properties to the part to address the variance in mechanical properties between layers.

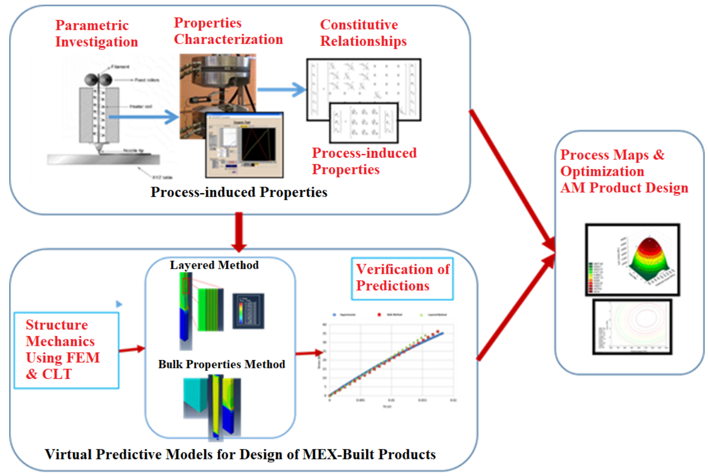

Figure 2: Schematic representation of the proposed investigative approach.

Stiffness Properties of MEX Thermoplastic Polymers

Tensile Properties

All testing panels were constructed in a STRATASYS FDM FORTUS 400mc system. Two build directions were used to determine all the required anisotropic properties. One group of panels was built flat (denoted as X-Y), and the second was built upright vertically (denoted as Z-X). All machine settings were set to the default values for ULTEM 9085. The extruder liquefier process temperature was at the default 375 °C for ULTEM 9085. The following special adjustments were made to the process parameters to maintain the integrity of the MEX printing process: (*i*) custom groups were created in the slicing software to force the internal fill raster to maintain the same angle at every layer, and (*ii*) the system mode “thin wall” was selected for the upright thin Z-X panels. This arrangement reduced the set printing enclosure temperature to 185 °C, decreasing the warping of tall, thin structures. The actual air temperatures at the build plane were approximately 10-15 °C cooler than the set-point of the printer.

The mechanical properties of the MEX-produced panels, at room temperature, were determined using an MTS load-frame equipped with a 5.0 KN load cell and a data acquisition system. The tension test was performed according with ASTM D638 standard test method for tensile properties of plastics at 5 mm/min. The strain data was recorded using tri-axis strain gages (WA-XX-060WR-120, Vishay) along the 0°, 45°, and 90° directions. Weight, length, width, and thickness measurements were recorded for each sample. Width measurements were taken at five different locations along the longitudinal axes of the samples. Figures 3-5 demonstrate how tensile properties of flat panels, with printed filaments oriented along, perpendicular, and 45° to the loading direction, are used to determine the elastic moduli along the in-plane principal axes. Major and minor Poisson’s ratios and shear moduli were also obtained from the same tests. The properties along the third principal axis were determined in the present work by testing the upright panels (Z-X) with different raster orientations to avoid the inaccuracy of the transverse isotropy assumption discussed above. Figure 6 displays the methods of estimating the values E_3, υ_{31}, and

υ_{32}. E_3 was obtained from the stress-strain curves. Poisson's ratios υ_{31} and υ_{32} were found using bidirectional strain gage rosettes. The ratio υ_{32} was obtained from the 0° samples and υ_{31} from the 90° (vertically built) Z-X samples.

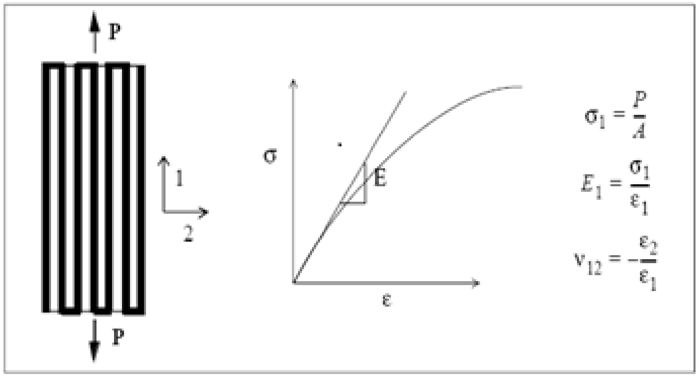

Figure 3: Anisotropic stiffness properties of flat panels X-Y with a raster angle of 0° [16].

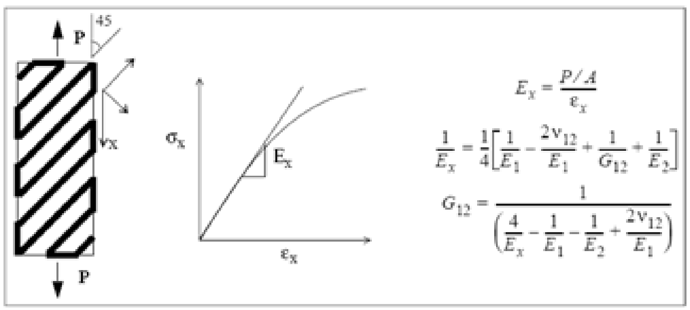

Figure 4: Anisotropic stiffness properties of flat panels X-Y with a raster angle of 90° [16].

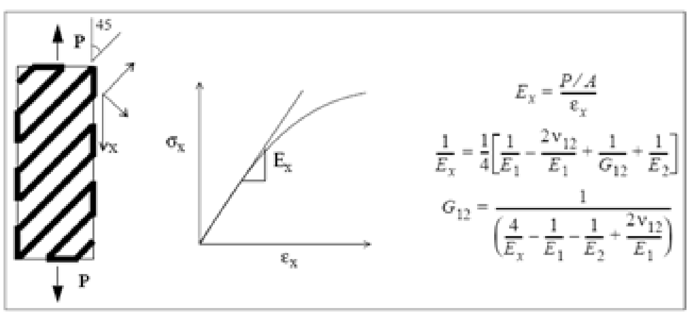

Figure 5: Anisotropic stiffness properties of flat panels X-Y with a raster angle of 45° [16].

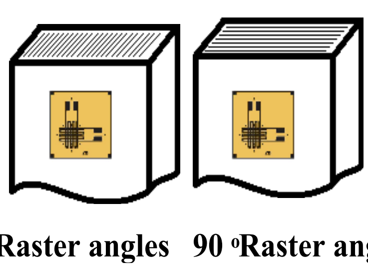

Figure 6: Measurements of E_3, υ_{31}, and υ_{32} using vertical panels Z-X.

Shear Properties

To directly determine the shear properties of ULTEM 9085 (instead of being commonly resolved indirectly from tensile testing), a specific testing procedure designed for composite materials was used herein using a specialized fixture (Wyoming Test Fixtures Inc.) per ASTM D5379. The test calls for ±45° shear strain gages (SA-06-125TK-350). The cord modulus (G_{12}, G_{13}, and G_{23}) was then determined by plotting the stress and strain data from a minimum of five samples. Figure 7 displays various shear test sample designs with different printing orientations, while Figure 8 depicts the shear experiment setup. Figure 8 shows a view of the Universal Testing Machine with the shear fixture used for testing the printed samples.

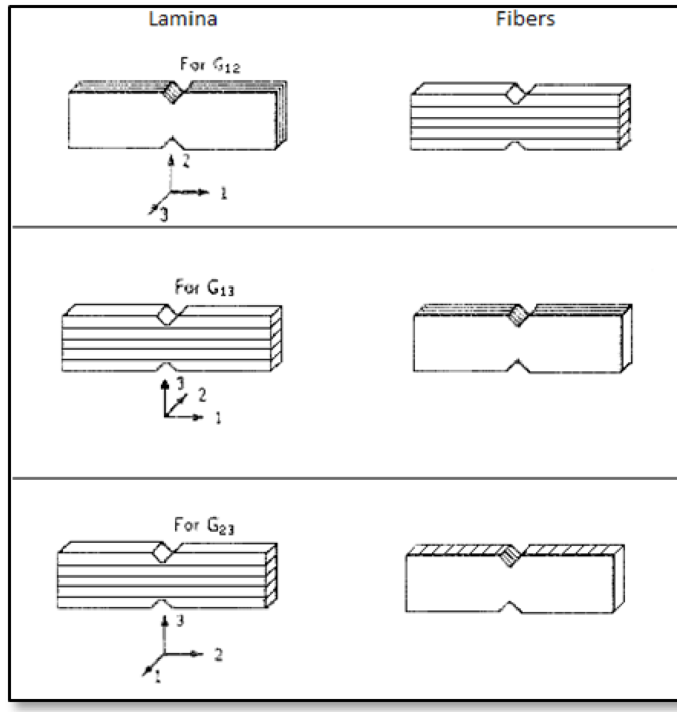

Figure 7: Shear samples designs with different printing orientations.

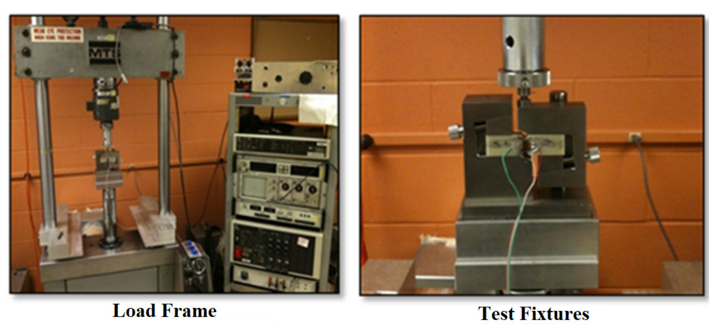

Figure 8: Shear testing setup for determination shear properties of 3D printed samples.

Structural Mechanics OF MEX-built Products

An analysis using the classical laminate theory (CLT) [31] was used to determine the anisotropic stiffness matrix for MEX-built parts. Each 3D printed layer (*i.e.*, lamina) is subjected to normal stresses σ_1, σ_2, and σ_3 and shear stresses τ_{23}, τ_{13}, and τ_{12}. These stresses are related to the corresponding strains by

$$\begin{Bmatrix} \varepsilon_1 \\ \varepsilon_2 \\ \varepsilon_3 \\ \gamma_{23} \\ \gamma_{13} \\ \gamma_{12} \end{Bmatrix} = \begin{bmatrix} 1/E_1 & -\upsilon_{21}/E_2 & -\upsilon_{31}/E_3 & 0 & 0 & 0 \\ -\upsilon_{12}/E_1 & 1/E_2 & -\upsilon_{32}/E_3 & 0 & 0 & 0 \\ -\upsilon_{13}/E_1 & -\upsilon_{23}/E_2 & 1/E_3 & 0 & 0 & 0 \\ 0 & 0 & 0 & 1/G_{23} & 0 & 0 \\ 0 & 0 & 0 & 0 & 1/G_{13} & 0 \\ 0 & 0 & 0 & 0 & 0 & 1/G_{12} \end{bmatrix} \begin{Bmatrix} \sigma_1 \\ \sigma_2 \\ \sigma_3 \\ \tau_{23} \\ \tau_{13} \\ \tau_{12} \end{Bmatrix} \quad (1)$$

where, E_1, E_2, and E_1 and are the elastic moduli and the Poisson's ratios are υ_{12}, υ_{21}, υ_{13}, υ_{31}, υ_{23}, and υ_{32} and the shear moduli are G_{12}, G_{13}, and G_{23}.

The assumption of plane stress allows for setting the stress components σ_3, τ_{23} and τ_{13} to zero and the 1-2 plane of the principal material coordinate system is in the plane of the layer (lamina), reducing the stress-strain relationship to

$$\begin{Bmatrix} \sigma_x \\ \sigma_y \\ \tau_{xy} \end{Bmatrix} = \begin{bmatrix} \bar{Q}_{11} & \bar{Q}_{12} & \bar{Q}_{16} \\ \bar{Q}_{12} & \bar{Q}_{22} & \bar{Q}_{26} \\ \bar{Q}_{16} & \bar{Q}_{26} & \bar{Q}_{66} \end{bmatrix} \begin{Bmatrix} \varepsilon_x \\ \varepsilon_y \\ \gamma_{xy} \end{Bmatrix} \quad (2)$$

Where, [Q] is the reduced stiffness matrix and, σ_x, σ_y, and τ_{xy} are the in-plane stresses, and ε_x, ε_y, and γ_{xy} are the corresponding in-plane strains.

Process-induced Properties and Constitutive Relationships Mechanical Properties of MEX-build ULTEM 9085

Data was collected as a function of raster orientations, ranging between 0° and 90° in increments of 15°, to understand the effect of raster angle on the mechanical behavior of MEX-printed materials. Additionally, the mechanical behavior of the injection molded parts was also collected for comparison. Figure 9 displays the stress-strain curves of all samples. The strength, ductility, and toughness of the injection molded samples were notably higher than the MEX-processed counterparts. The reported decrease in strength and ductility can be attributed to process-induced defects, including degraded inter-layer interfacial strength, air gaps between printed roads, and thermal gradient during printing. The relatively high printing temperature might also affect the macromolecule [2]; however, further research is required to substantiate the interrelationship of printing temperature and molecular structure of ULTEM 9085 during the MEX process.

Constitutive Equations for MEX-built Materials

Table 1 summarizes major mechanical properties obtained from tensile testing of MEX-printed ULTEM 9085 flat samples (X-Y) with 0°, 45°, and 90° raster angles. The results in Table 1 are the average from testing five panels for each orientation. Table 2 lists the major mechanical properties obtained from samples printed in the upright direction as a function of the same raster angles. Comparing the results in Tables 1 and 2 reveals that the strength and modulus of upright samples are lower by about 20%, on average than the flat counterparts.

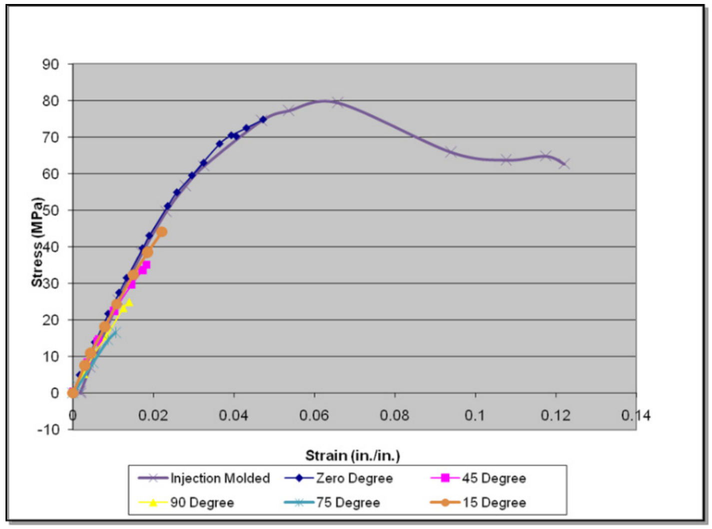

Figure 9: Stress-strain curves for MEX-built ULTEM 9085 flat panels with different raster angles, compared with properties of injection molded counterparts.

Table 1: Tensile mechanical properties of ULTEM 9085 extracted from flat panels.

Raster Angle	Elastic Modulus (MPa)	UTS* (MPa)	S_y* (MPa)	Elongation (%)
0°	2539 ± 104	78.6 ± 3.44	57.5 ± 4.60	4.38 ± 0.15
45°	2425 ± 166	56.76 ± 4.64	44.89 ± 4.14	3.31 ± 0.38
90°	2328 ± 178	45.70 ± 8.71	42.85 ± 6.19	2.37 ± 0.81

* UTS = Ultimate Tensile Strength and S_y = Yield Strength.

Table 2: Tensile properties of ULTEM 9085 extracted from tested upright panels.

Raster Angle	Elastic Modulus (MPa)	UTS (MPa)	S_y (MPa)	Elongation (%)
0°	2164 ± 27	52.0 ± 2.4	43.8 ± 2.3	2.79 ± 0.2
45°	2171 ± 121	51.9 ± 5.8	45.5 ± 1.7	2.7 ± 0.4
90°	1992 ± 92	54.3 ± 1.4	43.7 ± 0.8	3.4 ± 0.1

The data listed in Tables 1 and 2 could be aggregated based on approximate shear properties under the assumption of transverse isotropy but at the cost of inaccuracy. The shear properties are reported in Table 3. The results in this table also compare the predictions using Kulkarni et al. [16] analytical approach assuming transverse anisotropy and experimentally measured values herein, elucidating the large difference between the approaches, particularly for E_3, υ_{13}, υ_{23}, G_{12}, and G_{13}. The results indicate slight differences with the experimental measurements, about 8%, in calculating E_3, representing Young's moduli of a layer along the principal axes 3. Differences concerning shear moduli, G_{12}, and G_{13}, reached a 50% level, while it was minimal for G_{23} with merely a 3% difference. Concerning Poisson's ratios, the difference with experimental measurements reached a significant level of 45% for υ_{23} and only 15% for υ_{13}.

Table 3: Comparison between stiffness of ULTEM 9085 using predicted values based on Kulkarni et al. [16] and the presented experimental approach showing significant differences.

Property	Predicted Values	Experimental Values	Deviation
E_1	-	2540 MPa	
E_2	-	2330 MPa	
E_3	2330 MPa	2160 MPa	8%
υ_{12}	-	0.46	
υ_{13}	0.46	0.40	15%
υ_{23}	0.58	0.40	45%
G_{12}	840 MPa	560 MPa	50%
G_{13}	840 MPa	560 MPa	50%
G_{23}	740 MPa	760 MPa	3%

Detailed Presentation and Verification of the Introduced Virtual Models

In this section, we verified the previously introduced methods using a test case scenario of tensile bars (ASTM D638-03). The width, thickness, and overall length of the tensile bars were 25.4, 3.2, and 254 mm, respectively. STRATASYS (the process developer) provided all tolerances on additively manufactured samples with a lower limit of ±0.2mm. The tensile bars used in this case scenario were printed in the flat (X-Y) and edge (X-Z) orientations (Figure 10) based on a twofold rationale. The results were used to (1) contrast the analysis methods in predicting the mechanical performance of the parts as a function of the build orientations and (2) determine possible performance variations. The tensile bars were fabricated with repeated [0, +60, -60 degrees] raster pattern layers These raster angle patterns are favored by the aerospace industry (Boeing Co., Saint Louis, MO). All the samples were also printed using polyetherimide (ULTEM 9085) due to its superior mechanical and physical properties compared with the commonly MEX-printed thermoplastics. The stiffness properties of MEX-processed ULTEM 9085 were determined using the procedures described in the previous section, which are summarized in Table 3.

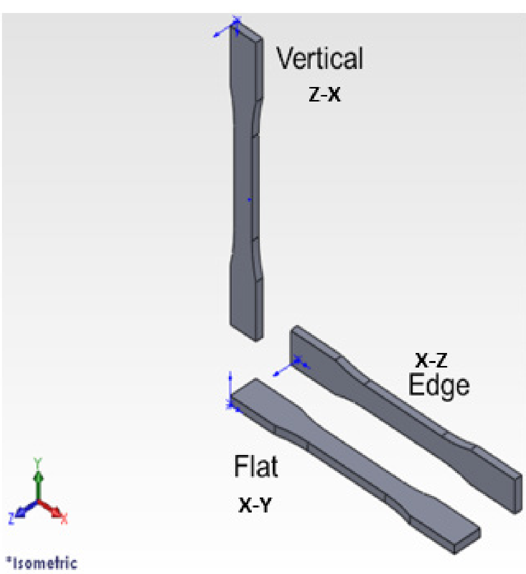

Figure 10: Printing orientations explored in test case scenario studies.

Layered Method

The layered method uses the ANSYS Composite Pre-Post (ACP) internal features of the finite element software to partition the part into several cells, each representing a single 3D printed layer. Several approaches could be used for partitioning, including sketching the boundaries or using datum features. Creating the datum planes as boundaries is reasonably straightforward by first identifying the face or plane of the part that corresponds to the initial printed layer. This face/plane is referenced to create parallel planes with an offset dimension equal to the layer thickness (*e.g.*, the slice height). Figure 11 displays the datum planes and partitioned cells for a tensile bar test case created by ACP module within the Ansys environment. Once all the partitions have been created, the layer orientations can be applied by defining the corresponding rotation angle using a user-specified coordinate system. An example of the applied material direction is shown in Figure 12, where the green arrows present the raster angles.

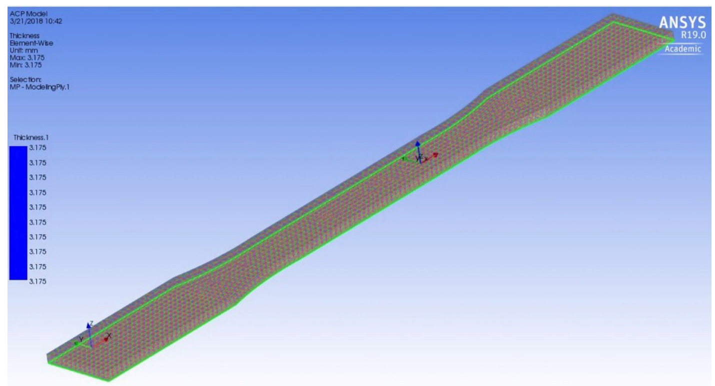

Figure 11: Datum planes displayed on a tensile bar as a green line for a flat (X-Y) build.

The resolved stresses for a flat (X-Y) tensile specimen using the layered method are shown in Figure 13. The figure provides a detailed view of the Mises stress variations among the discretized MEX layers.

In the current scenario, a fixed boundary was ascribed to one end of the tensile bar, and the load was applied to the other. An additional boundary condition was applied to simulate the action of the grippers by fixing two regions (25.4 mm) on either end of the tensile bar while still allowing deformation along the line of pull to prevent twisting motion. The yield strength for ULTEM 9085 was derived from the corresponding experimental data. The truest representation of a tensile test would be to ramp the load from 0 to the maximum. However, because ANSYS converges to a solution by ramping the applied load, creating the maximum load condition was sufficient.

Bulk Properties Method

The classical laminate theory (CLT) [25] determines the bulk mechanical properties of a composite part by transforming the property values from the local coordinate system of each layer (1: along the fiber; 2: orthogonal to the fiber; interlayer, and 3: orthogonal to the fiber, interlayer) to the global coordinate system

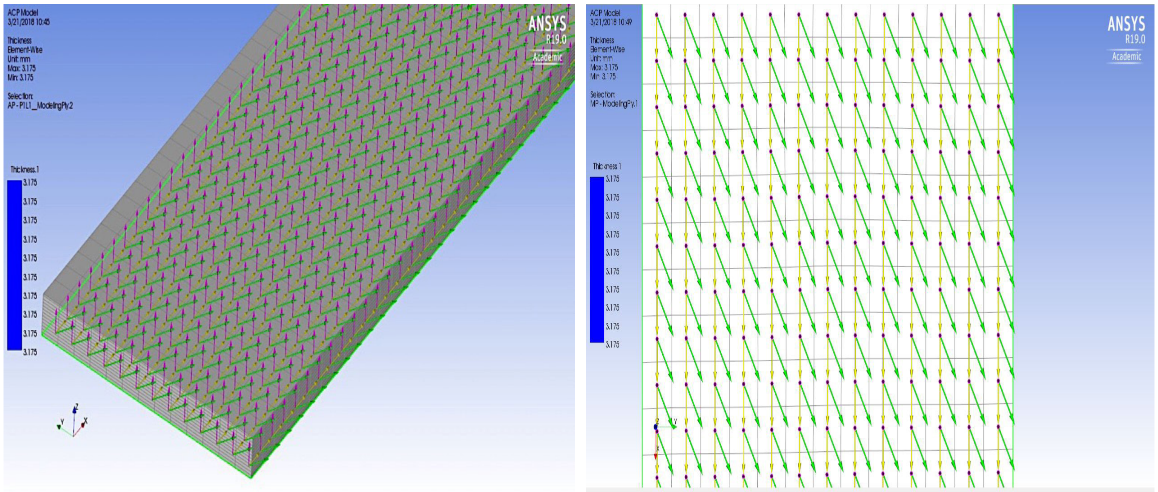

Figure 12: Selected layers and their local material orientations (isometric and top views).

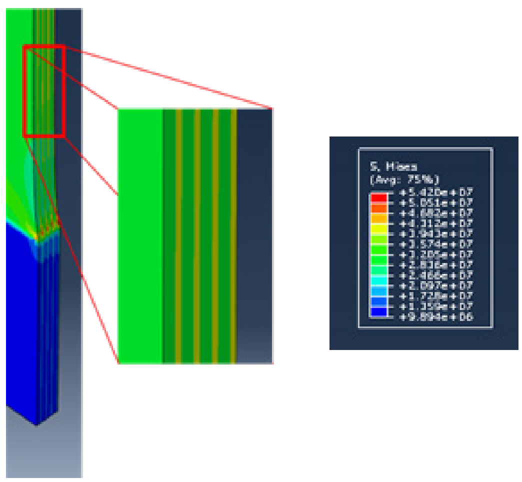

Figure 13: Stress variation detail (high stress regions are 0° layers and low stress regions are ±60° layers).

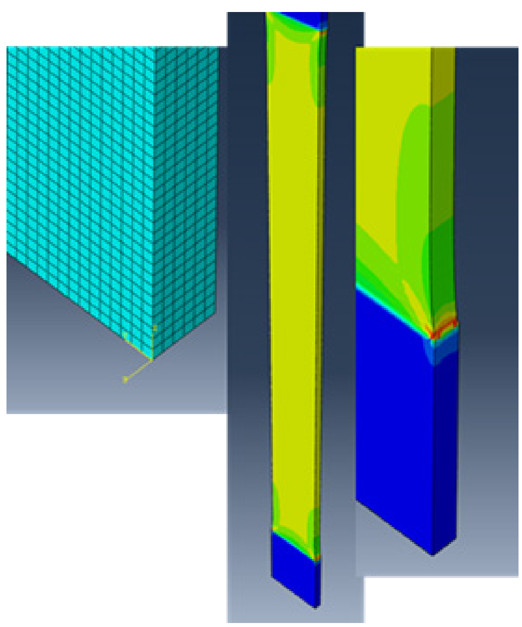

Figure 14: Meshing, and simulation results of Von Mises Stress distribution using bulk properties method.

of the part. The bulk properties method employs this technique, where the varying orientation of the MEX layers is handled mathematically. The following assumptions are considered for the bulk properties approach:

- Each layer (lamina) is quasi-homogeneous and orthotropic,
- Displacements are continuous throughout the laminate,
- The laminate is treated as a state of plane stress, and
- The engineering constants of unidirectional layer are given.

The resolved Von Misses stresses for a flat (X-Y) tensile specimen using bulk properties method are shown in Figure 14. The figure provides a detailed view of the Mises stress variations among the discretized MEX printed part. Notably, the bulk properties method produces a uniform stress throughout the thickness of the part along gage length (deformed zone) since the mechanical attributes are homogenized throughout the part.

Verification of the Introduced Virtual Models

This section compares the results from experimental tensile tests, the predication bulk properties method, and forecast from the layered method. The experimental data is the average of three samples. Figure 15a depicts the results for the flat (X-Y) specimens, and Figure 15b displays the results for the edge-built (X-Z) specimens.

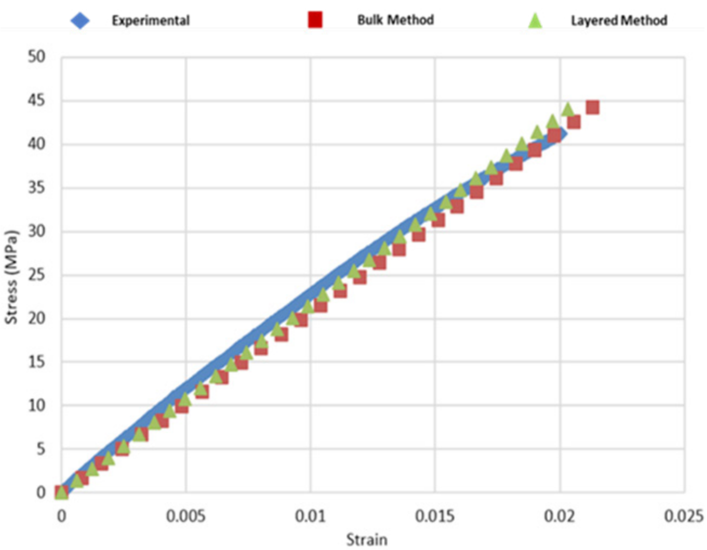

Figure 15: Comparison of experimental and numerical results for a flat (X-Y) built part.

Based on the results in Figure 14, most of the discrepancies between the numerical and experimental results can be attributed to the tensile bars being pulled until yielding above the elastic behavior. However, analytical and computational methods predicted the deformation behavior with favorable accuracy (<10% deviation) compared to the nearly linear portions of the experimental data. A negligible difference is noted between the results of the layered and bulk properties methods (< 0.1%). The stress-strain plots proved that both methods were accurate in modeling the differing properties resulting from a multi-layered, multi-directional composite-like structure. Overly conservative estimations (such as applying the lowest Young's modulus to an isotropic material model) were also undesirable since optimization based on weight minimizing is a common objective in industrial applications. Thus, the layered and bulk properties methods used in this work provide viable solutions for modeling MEX-based parts. Additionally, the similarity of the results of the methods offers future developers and designers a choice depending on the needs of the analysis. Although the layered method is significantly slower, it also details the stress in each individual layer as a function of the printing orientation.

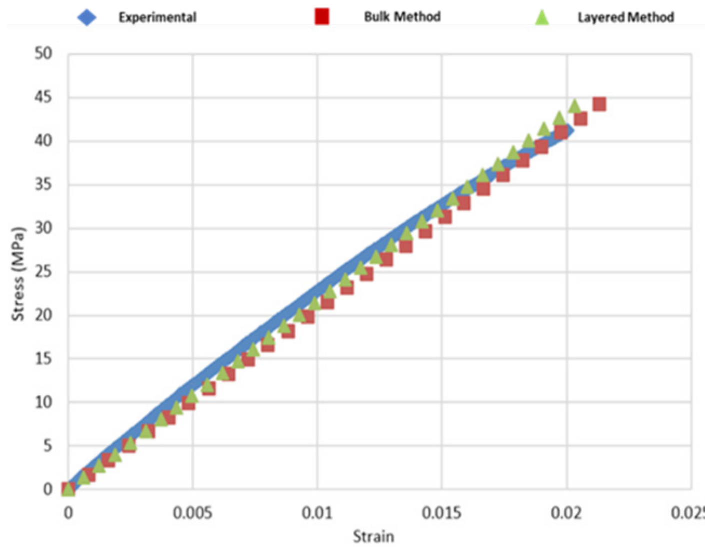

Figure 16: Comparison of experimental and numerical results for edge (X-Z) built parts.

Figure 15 displays comparison of experimental and numerical results for the flat (X-Y) built part, while, Figure 16 presents comparison of experimental and numerical results for the edge (X-Z) built part. Based on the results in Figures 15 and 16, most of the discrepancies between the numerical and experimental results can be attributed to the tensile bars being pulled until yielding above the elastic behavior. However, analytical and computational methods predicted the deformation behavior with favorable accuracy (<10% deviation) compared to the nearly linear portions of the experimental data. A negligible difference is noted between the results of the layered and bulk properties methods (< 0.1%). The stress-strain plots proved that both methods were accurate in modeling the differing properties resulting from a multi-layered, multi-directional composite-like structure. Overly conservative estimations (such as applying the lowest Young's modulus to an isotropic material model) were also undesirable since optimization based on weight minimizing is a common objective in industrial applications. Thus, the layered and bulk properties methods used in this work provide viable solutions for modeling MEX-based parts. Additionally, the similarity of the results of the methods offers future developers and designers a choice depending on the needs of the analysis. Although the layered method is significantly slower, it also details the stress in each individual layer as a function of the printing orientation.

Conclusions

The emergence of material extrusion as a viable additive manufacturing process for producing load-bearing parts made of ULTEM 9085 necessitates accelerating the development and deployment cycle by transcending current heuristic design approaches. This research presents an integrated approach for quantifying process-induced properties by effectively utilizing the measured properties within a predictive analysis framework tailored to design MEX-printed products. Samples fabricated with different printing orientations were tested in tension and shear to extract the mechanical properties as a function of processing parameters. The experimental properties of the 3D printed parts were inferior to the injection molding counterparts due to process-induced anisotropy and manufacturing artifacts. The analysis paradigm consisted of two methods: numerical based on finite element analysis and analytical based on classical lamination theory. The motivation for adopting these methods stems from the analogy between MEX-based and composite materials structure due to the layer-by-layer production framework in additive manufacturing and fiber-reinforced composites. The analysis procedures are proven interchangeable, affording developers and designers the choice based on the application and analysis requirements. Although the discrepancy between the two approaches is insignificant, the increase in the geometrical complexity and printing configurations may favor one method over another. Further investigation into this behavior should be conducted to determine the significance of these effects, considering different geometries and application requirements while considering the dominant failure mechanisms as a function of loading.

Acknowledgments

The authors wish to acknowledge the in-kind support provided by The Boeing Company, STRATASYS, Inc., and ITECH D&M, LLC, for this research. Our appreciation is also extended to Mr. Gregg R. Bogucki and Mr. Michael Hayes of Boeing Research and Technology and Mr. Jeffery DeGrange (Former Vice President) of STRATASYS for their technical advice and encouragement during the present work. We acknowledge also, the early work provided by Dr. Thao T. P. Phan, and Dr. Brian Graybill, University of Missouri, for establishing the methodology for testing mechanical properties of MEX printed polymer samples.

References

1. Killi SW. Additive manufacturing: design, methods, and processes. CRC Press. 2017; 254.
2. Youssef G, Applied mechanics of polymers: properties, processing, and behavior. Elsevier. 2021.
3. Gebisa AW, Lemu HG. Effect of process parameters on compressive properties of ULTEM 9085 produced by FDM process. in ASME International Mechanical Engineering Congress and Exposition. The American Society of Mechanical Engineers. 2018.
4. Schöppner V, Bagsik A. Mechanical properties of fused deposition modeling parts manufactured with ULTEM*9085. ANTEC. 2011; 1294-1298.
5. Zaldivar RJ, Witkin DB, McLouth T, et al. Influence of processing and orientation print effects on the mechanical and thermal behavior of 3D-Printed ULTEM® 9085 Material. Additive Manufacturing. 2017: 13: 71-80.
6. Gebisa AW, Lemu HG. Influence of 3D printing FDM process parameters on tensile property of ULTEM 9085. Procedia Manufacturing. 2019; 30: 331-338.
7. Vakharia VS, Leonard H, Singh M, et al. Multi-Material Additive Manufacturing of High Temperature Polyetherimide (PEI)–Based Polymer Systems for Lightweight Aerospace Applications. Polymers. 2023; 15: 561.
8. Gibson I, Rosen D, Stucker B, et al. Additive manufacturing technologies. Springer. 2021; 17.
9. Turner BN, Strong R, Gold SA. A review of melt extrusion additive manufacturing processes: I. Process design and modeling. Rapid prototyping journal. 2014; 20: 192-204.
10. Moon SK, Tan YE, Hwang J, et al. Application of 3D printing technology for designing light-weight unmanned aerial vehicle wing structures. International Journal of Precision Engineering and Manufacturing-Green Technology. 2014; 1: 223-228.
11. Pecho P, Azaltovic V, kandera B, et al. Introduction study of design and layout of UAVs 3D printed wings in relation to optimal lightweight and load distribution. Transportation Research Procedia. 2019; 40: 861-868.
12. Bacciaglia A, Ceruti A, Liverani A. A design of experiment approach to 3D-printed mouthpieces sound analysis. Progress in Additive Manufacturing. 2021; 6: 571-587.
13. Qiao D, Wang B, Gu H. Additive Manufacturing: Challenges and Solutions for Marine and Offshore Applications. International Conference on Offshore Mechanics and Arctic Engineering. American Society of Mechanical Engineers. 2020; 7.
14. Zhang L, Chen X, Zhou W, et al. Digital Twins for Additive Manufacturing: A State-of-the-Art Review. Applied Sciences. 2020; 10: 8350.
15. Knapp GL, Mukherjee T, Zuback JS, et al. Building blocks for a digital twin of additive manufacturing. Acta Materialia. 2017; 135: 390-399.
16. Kulkarni P, Dutta D. Deposition Strategies and Resulting Part Stiffnesses in Fused Deposition Modeling. J. Manuf. Sci. Eng. 1999; 121: 93-103.
17. Yardimci AM, Guceri SI, Danforth SC, et al. Numerical modeling of fused deposition processing. Proceedings of the 1995 ASME International Mechanical Congress and Exposition. 1995; 1225-1235.
18. Pennington RC, Hoekstra NL, Newcomer JL. Significant factors in the dimensional accuracy of fused deposition modelling. Proceedings of the Institution of Mechanical Engineers, Part E: Journal of Process Mechanical Engineering. 2005; 219: 89-92.

19. Phan TTP, Phan TQ, El-Gizawy AS. Development of a combined analytical and experimental approach for the determination of the cohesive strength between material extrusion layers using the true area of contact. Additive Manufacturing. 2019; 30: 100832.

20. Huynh NU, Smilo J, Blourchian A, et al. Property-map of epoxy-treated and as-printed polymeric additively manufactured materials. International Journal of Mechanical Sciences. 2020; 181: 105767.

21. Youssef G, Smilo J, Blourchian A, et al. Multifunctional fused deposition modeled acrylonitrile butadiene styrene-based structures with embedded conductive channels. J. Eng. Mater. Technol. 2021; 143: 011001.

22. Zhang Y, Chou YK. Three-dimensional finite element analysis simulations of the fused deposition modelling process. Proceedings of the Institution of Mechanical Engineers, Part B: Journal of Engineering Manufacture. 2006; 220: 1663-1671.

23. Zhang Y, Chou K. A parametric study of part distortions in fused deposition modelling using three-dimensional finite element analysis. Proceedings of the Institution of Mechanical Engineers, Part B: Journal of Engineering Manufacture. 2008; 222: 959-968.

24. Ahn SH. Anisotropic tensile failure model of rapid prototyping parts-fused deposition modeling (FDM). International Journal of Modern Physics B. 2003; 17: 1510-1516.

25. Daniel IM, Ishai O. Engineering mechanics of composite materials. Oxford university press. 1994, 2006.

26. Domingo-Espin M, Puigoriol-Forcada JM, Garcia-Granada AA, et al. Mechanical property characterization and simulation of fused deposition modeling Polycarbonate parts. Materials & Design. 2015; 83: 670-677.

27. Sood AK, Ohdar RK, Mahapatra SS. Parametric appraisal of mechanical property of fused deposition modelling processed parts. Materials & Design. 2010; 31: 287-295.

28. Rodrıguez JF, Thomas JP, Renaud JE. Design of fused-deposition ABS components for stiffness and strength. J. Mech. Des. 2003; 125: 545-551.

29. Shah JR, Thanki S. Investigation of the Tensile Properties in Continuous Glass Fiber–Reinforced Thermoplastic Composite Developed Using Fused Filament Fabrication. Journal of Testing and Evaluation. 2023; 51: 20220643.

30. Tommy H, Richard M, Rich F. Design of Coupons and Test Methodology for Orthotropic Characterization of FFF-Processed Ultem 9085. Fourth ASTM Symposium on Structural Integrity of Additive Manufactured Materials and Parts. ASTM International. 2020.

31. Özen A, Auhl D. Modeling of the mechanical properties of fused deposition modeling (FDM) printed fiber reinforced thermoplastic composites by asymptotic homogenization. Composites and Advanced Materials. 2022; 31: 1-13.

32. Özen A, Abali BE, Vollmecke C, et al. Exploring the role of manufacturing parameters on microstructure and mechanical properties in fused deposition modeling (FDM) using PETG. Applied Composite Materials. 2021; 28: 1799-1828.

33. Cuan-Urquizo E, Barocio E, Tejada-Ortigoza V, et al. Characterization of the mechanical properties of FFF structures and materials: A review on the experimental, computational and theoretical approaches. Materials. 2019; 12: 895.